Journal of Applied Polymer Science

Cracking energy density calculation of hyperelastic constitutive model and its application in rubber fatigue life estimations

Yanhua Peng,[1] Guixiong Liu,[1] Yanming Quan,[1] Qilin Zeng[2]

[1]School of Mechanical and Automotive Engineering, South China University of Technology, Guangzhou 510640, People's Republic of China

[2]SCUT Bestry Technology Co, Ltd, Guangzhou 510640, People's Republic of China

Correspondence to: G. X. Liu (E-mail: megxliu@scut.edu.cn)

ABSTRACT: The finite deformation of rubber under multiaxial stress will finally result in its fatigue failure. The ability to predict the effects of complex strain histories on fatigue life is a critical need. The cracking energy density (CED) distribution characteristics in the finite deformation and rubber fatigue life estimated by the CED criterion are investigated. Then the influences of the crack orientation angle θ and the principal stretch ratio λ on the relationship between CED and strain energy density (SED) are obtained. Finally, the results are used for predicting the fatigue life of rubber material and are compared to experimental values. The results indicate that the ratios of the predicted lives based on the CED damage parameter and measured lives are within two times scatter factor and that of the predicted lives based on the SED damage parameter and measured lives are greatly influenced by the crack orientation angle θ. The rubber fatigue life has great relationship with the angle of the crack plane normal vector and the first principal stretch direction. © 2016 Wiley Periodicals, Inc. J. Appl. Polym. Sci. **2016**, *133*, 44195.

KEYWORDS: manufacturing; mechanical properties; rubber

Received 21 March 2016; accepted 19 July 2016
DOI: 10.1002/app.44195

INTRODUCTION

Owing to its superior ability to withstand large strains without permanent deformations, rubber is widely used in tires, seals, vibration isolators, medical apparatuses, and instruments etc.[1] In recent years, many researchers have investigated the fatigue life of rubber materials or rubber artifacts, respectively from the loading process,[2–5] working environment,[6,7] the optimization of rubber material and formula and rubber constitutive response of dissipation etc.[8,9] In the actual working conditions, rubber components are often operate under multiaxial loading status.[10–13] Mars, Fatemi, Zine, and Ayoub *et al.* investigated the multiaxial fatigue life of natural rubber (NR) and styrene butadiene rubber (SBR) on load ratio R, axial or torsional load, maximum and minimum loads, average load, load sequence, and load frequency etc.[1,2,4,11,13] Mars studied traditional equivalent parameters of multiaxial fatigue life, and put forward the cracking energy density (CED) criterion for the first time.[5]

Finite element simulation technology plays an important role in the study of rubber fatigue.[10,14] Several researchers proposed a variety of hyperelastic constitutive models through experiments and theoretical analysis of specific rubber formula or specimen.[15–17] Typical models include Neo-Hooke model, Mooney Rivlin model, Yeoh model and Ogden model.[16] The studies found that the representational capacity of the mechanical properties different hyperelastic constitutive models is varied with different formulae.[18] Considering its strong adaptability in engineering and sufficient accuracy in calculation,[19] the Ogden model is usually adopted.[20]

On the one hand, as the requirements of mechanical properties of rubber products for consumers become more demanding, the differences of mechanical properties characterization ability cannot be ignored by different constitutive models. On the other hand, through multiple fatigue tests to dumbbell simple tension specimens, dumbbell cylindrical specimens and hollow cylindrical specimens, Shangguan *et al.*[21] concluded that the relationships between the tension fatigue life and the damage parameters are geometry-independent and the fatigue life is primarily dependent upon the material properties. This discovery makes it possible to simplify the structure of a variety of complex rubber components. Therefore, the crack orientation angle and the principal stretch ratio have important application value in the multiaxial fatigue research.

In this paper, the multiaxial fatigue life of rubber finite deformation based on the CED criterion is investigated by the crack growth approach. As the crack orientation angle θ and the principal stretch ratio λ change, the ratio of CED and SED are

calculated under several typical stress–strain states. Meanwhile the influence of the Ogden model order to the ratio of CED and SED are discussed. Then the predicted life based on SED criterion and the relationships of CED and SED are used to estimate the fatigue life of rubber based on CED criterion. Finally, the predicted fatigue lives will be compared with the experimental values.

CED CALCULATION BASED ON CONSTITUTIVE RELATION UNDER FINITE STRAIN

Under multiaxial fatigue loading, not all SED is used for driving the crack propagation. The available portion of SED actually to drive the crack propagation is CED. The relationship between CED and SED under small strain is concluded in eq. (1)[5]:

$$\frac{W_c}{W}=\frac{[2Bv^2+(2-B)v-1]\cos^2\theta+[B(B+v)(2v-1)]\sin^2\theta}{[2Bv^2+(2-B)v-1]+[B(B+v)(2v-1)]} \quad (1)$$

where $B=\frac{\ln\lambda_2}{\ln\lambda_1}$; v is the Poisson ratio.

On this basis, Zine *et al.* studied the CED of the simplest Neo-Hookean model under conditions of finite strain.[11] Such a constitutive law can only describe unfilled rubber mechanical behaviors generally well. However, adding formula in rubber might strongly modify its mechanical behaviors, which is a necessary process to enhance the mechanical properties. Thus, more constitutive laws of incompressible rubber-like materials and the corresponding finite element analysis methods are required in studies of mechanical properties of rubber materials.[11,21]

The CED under Finite Strain

In finite deformation of rubber material, the direction of the crack growth is usually decided by the local stress and strain direction around the initial defect. Figure 1 describes a potential crack surface. While the relationship between the crack plane and load direction is uncertain, potential crack plane direction may be any direction from Point O to the sphere. Assuming the coordinates of the arbitrary point on the sphere is (x, y, z). Thus,

$$\begin{cases} x=\sin\omega.\cos\gamma \\ y=\sin\omega.\sin\gamma, 0\le\omega\le\pi, 0\le\gamma\le2\pi \\ z=\cos\omega \end{cases}$$

where ω is the angle between vector $\boldsymbol{R}$ and the Z-axis; γ is the angle between vector $\boldsymbol{R}$ projection in the XY plane and the X-axis;$\boldsymbol{R}=[x, y, z]^T$; and$|\boldsymbol{R}|=1$. In the rubber crack propagation, the increment of CED which drives the crack initiation and propagation effectively can be calculated as follows:

$$dW_c=\boldsymbol{\sigma}.d\varepsilon=\boldsymbol{\sigma}.\boldsymbol{D}dt \quad (2)$$

where $d\varepsilon$ is the strain increment vector; $\boldsymbol{\sigma}$ is stress vector; $\boldsymbol{D}$ is deformation rate vector.

Under nonlinear finite strain conditions, the influence of coordinate deformation must be considered while predicting the location and direction of fatigue cracks. After the undeformed face element transforms to be deformed, its normal vector changes accordingly. Then, the increment of CED dW_c is expressed as:

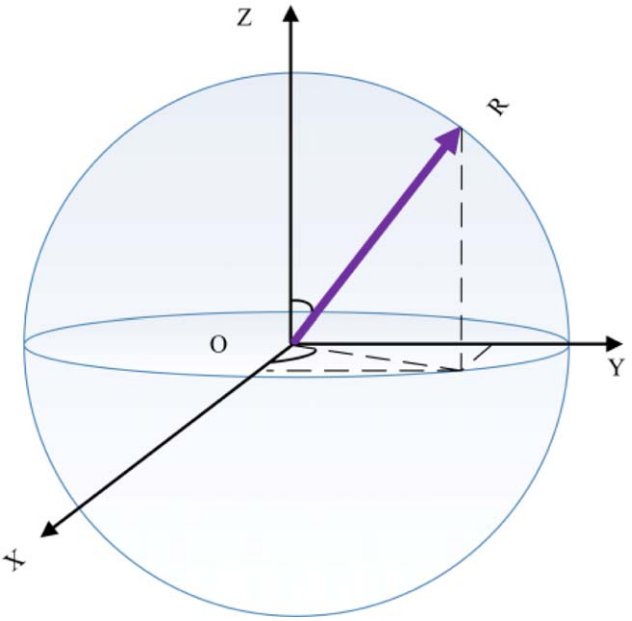

Figure 1. Unit sphere representing all possible crack normal vectors in the undeformed state. [Color figure can be viewed at wileyonlinelibrary.com.]

$$dW_c=J^{-1}\frac{\boldsymbol{R}^{\mathrm{T}}\boldsymbol{S}d\boldsymbol{E}\boldsymbol{C}^{-1}\boldsymbol{R}}{\boldsymbol{R}^{\mathrm{T}}\boldsymbol{C}^{-1}\boldsymbol{R}} \quad (3)$$

where $J=\frac{\rho_0}{\rho}$ is the ratio of the undeformed mass density to the deformed mass density; $\boldsymbol{S}$ is the second Piola-Kirchhoff stress tensor; $\boldsymbol{E}$ is the Green-Lagrange strain tensor; $\boldsymbol{C}$ is the right Cauchy-Green deformation tensor. The relationship between Green-Lagrange strain tensor and the right Cauchy-Green deformation tensor is as follows:

$$\boldsymbol{E}=\frac{\boldsymbol{C}-\boldsymbol{I}}{2} \quad (4)$$

where $\boldsymbol{I}$ is the unit tensor. The right Cauchy-Green deformation tensor $\boldsymbol{C}$ and the principal stretch ratio λ are related by:

$$\boldsymbol{C}=\sum_{j=1}^{3}\lambda_j^2\boldsymbol{e}_j\otimes\boldsymbol{e}_j\ \ (j=1,2,3) \quad (5)$$

$\boldsymbol{e}_j$ is the normalized feature vector of the principal stretch direction. In Figure 2, assuming the angle of the crack plan normal vector with the first principal stretch direction is θ. If $\vec{\boldsymbol{R}}_\theta=[l_1, l_2, l_3]^T$ and $\sum_{j=1}^{3}l_j^2=1$, under plane stress state, $\vec{\boldsymbol{R}}_\theta=[\cos\theta, \sin\theta, 0]^T$.

The increment of CED dW_c, the second Piola-Kirchhoff stress tensor $\boldsymbol{S}$ and the right Cauchy-Green deformation tensor $\boldsymbol{C}$ are related by[4]:

$$dW_c=J^{-1}\frac{\vec{\boldsymbol{R}}_\theta{}^{\mathrm{T}}\boldsymbol{S}d\boldsymbol{C}\boldsymbol{C}^{-1}\vec{\boldsymbol{R}}_\theta}{2\vec{\boldsymbol{R}}_\theta{}^{\mathrm{T}}\boldsymbol{C}^{-1}\vec{\boldsymbol{R}}_\theta} \quad (6)$$

Assuming the deformation gradient tensor $\boldsymbol{F}=\mathrm{diag}(\ldots,\lambda_j,\ldots)$, j = 1, 2, 3. The Cauchy stress tensor $\boldsymbol{\sigma}$ and the second Piola-Kirchhoff stress tensor $\boldsymbol{S}$ are related by:

$$\boldsymbol{S}=J\boldsymbol{F}^{-1}\boldsymbol{\sigma}\boldsymbol{F}^{-T} \quad (7)$$

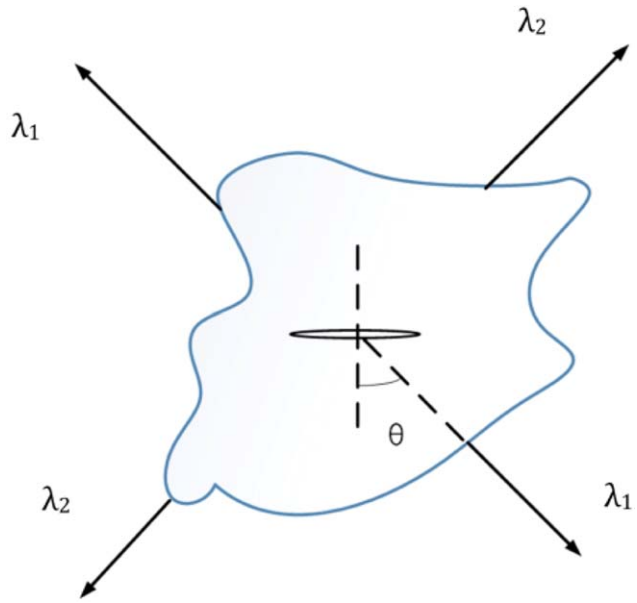

Figure 2. The domain with an arbitrary crack under stress. [Color figure can be viewed at wileyonlinelibrary.com.]

For incompressible materials $J=1$, the second Piola-Kirchhoff stress tensor $\boldsymbol{S}$ is as follows[22]:

$$\boldsymbol{S} = -p\boldsymbol{C}^{-1} + 2\frac{\partial W(\boldsymbol{C})}{\partial(\boldsymbol{C})} \tag{8}$$

Accordingly, the second Piola-Kirchhoff stress tensor $\boldsymbol{S}$ and the principal stretch ratio λ are related by:

$$S_j = -p\lambda_j^{-2} + \frac{1}{\lambda_j}\frac{\partial W}{\partial(\lambda_j)} \tag{9}$$

In plane stress state, hydrostatic pressure $\boldsymbol{p}$ value is decided by boundary conditions, when $S_3=0$ and $p=\lambda_3\frac{\partial W}{\partial(\lambda_3)}$. The increment of CED dW_c is as follows:

$$dW_c = \frac{\lambda_1 S_1 {l_1}^2}{{l_1}^2 + \left(\frac{\lambda_2}{\lambda_1}\right)^{-2}{l_2}^2}d\lambda_1 + \frac{\lambda_2 S_2 {l_2}^2}{{l_1}^2 + \left(\frac{\lambda_2}{\lambda_1}\right)^{-2}{l_2}^2}d\lambda_2 + \frac{-\left(\frac{\lambda_2}{\lambda_1}\right)^{3}{\lambda_1}^4 S_2 {l_2}^2}{{l_1}^2 + \left(\frac{\lambda_2}{\lambda_1}\right)^{-2}{l_2}^2}d\lambda_3 \tag{10}$$

CED Characterization Based on Ogden Model

The SED of Ogden model,[17] a function of the principal stretches λ_1, λ_2 and λ_3, is expressed as follows:

$$W = \sum_{i=1}^{N}\frac{\mu_i}{\alpha_i}\left(\lambda_1^{\alpha_i} + \lambda_2^{\alpha_i} + \lambda_3^{\alpha_i} - 3\right) + \sum_{i=1}^{N}\frac{1}{D_i}(J-1)^{2i} \tag{11}$$

In plane stress state, hydrostatic pressure $\boldsymbol{p}$ value of Ogden model is expressed as follows:

$$p = \sum_{i=1}^{N}\mu_i\lambda_3^{\alpha_i} \tag{12}$$

By eqs. (9) and (11), the second Piola-Kirchhoff stress tensor $\boldsymbol{S}$ of Ogden model in the principal stretch is expressed as follows:

$$S_1 = -\frac{1}{\lambda_1^2}\sum_{i=1}^{N}\mu_i\left(\frac{1}{\beta\lambda_1^2}\right)^{\alpha_i} + \sum_{i=1}^{N}\mu_i\lambda_1^{\alpha_i-2} \tag{13}$$

$$S_2 = -\frac{1}{(\beta\lambda_1)^2}\sum_{i=1}^{N}\mu_i\left(\frac{1}{\beta\lambda_1^2}\right)^{\alpha_i} + \sum_{i=1}^{N}\mu_i(\beta\lambda_1)^{\alpha_i-2} \tag{14}$$

Substituting eqs. (13) and (14) into eq. (10), if

$$A_1 = \frac{\lambda_1\left[-\frac{1}{\lambda_1^2}\sum_{i=1}^{N}\mu_i\left(\frac{1}{\beta\lambda_1^2}\right)^{\alpha_i} + \sum_{i=1}^{N}\mu_i\lambda_1^{\alpha_i-2}\right]\cos^2\theta}{\cos^2\theta + \beta^{-2}\sin^2\theta} \tag{15}$$

$$A_2 = \frac{\beta\lambda_1\left[-\frac{1}{(\beta\lambda_1)^2}\sum_{i=1}^{N}\mu_i\left(\frac{1}{\beta\lambda_1^2}\right)^{\alpha_i} + \sum_{i=1}^{N}\mu_i(\beta\lambda_1)^{\alpha_i-2}\right]\sin^2\theta}{\cos^2\theta + \beta^{-2}\sin^2\theta} \tag{16}$$

$$A_3 = \frac{-\beta^3{\lambda_1}^4\left[-\frac{1}{(\beta\lambda_1)^2}\sum_{i=1}^{N}\mu_i\left(\frac{1}{\beta\lambda_1^2}\right)^{\alpha_i} + \sum_{i=1}^{N}\mu_i(\beta\lambda_1)^{\alpha_i-2}\right]\sin^2\theta}{\cos^2\theta + \beta^{-2}\sin^2\theta} \tag{17}$$

The CED of Ogden model is expressed as follows:

$$dW_c = A_1 d\lambda_1 + A_2 d\lambda_2 + A_3 d\lambda_3 \tag{18}$$

where the biaxial parameters $\beta=\frac{\lambda_2}{\lambda_1}$; $\lambda_2=\beta\lambda_1$; $\lambda_3=\frac{1}{\beta\lambda_j^2}$. The development of the differential eq. (18) can lead to an integral expression of W_c.

THE CED CHARACTERIZATION ANALYSIS

Parameter Identification of Mechanical Properties

After testing the mechanical properties of rubber material, the finite element software ABAQUS is used for material evaluation. In Figure 3, Mooney-Rivlin model (Poly-N1), Neo-Hooke model (R-Poly-N1), Yeoh model (R-Poly-N3), and Ogden model are used to simulate the mechanical properties of rubber. The least

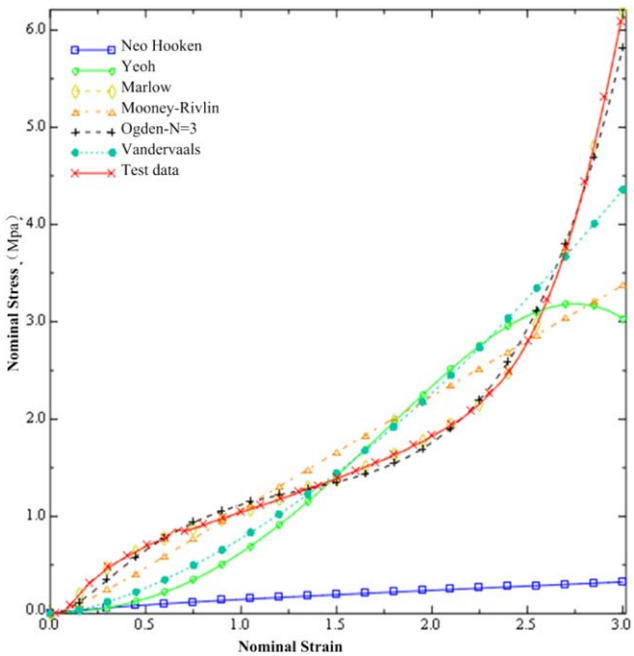

Figure 3. Material stress-strain curves of different hyperelastic constitutive model. [Color figure can be viewed at wileyonlinelibrary.com.]

Table I. The Material Fitting Parameters of Ogden Model ($N = 3$)

i	μ	α
1	1.349	1.367
2	−1.32e-7	−15.09
3	2.18e-5	12.29

Table II. Biaxial Parameter of Several Typical Strain States

Strain state	Biaxial parameter β
Uniaxial tensile (UT)	$\beta=\lambda^{-\frac{3}{2}}$
Planar tensile/pure shear (PT/PS)	$\beta=\lambda^{-1}$
Simple shear (SS)	$\beta=\lambda^{-2}$
Biaxial tensile (BT)	$\beta=\lambda_2\times\lambda_1^{-1}$

square method is used for the stress–strain curve fitting and obtaining material parameters. As it can be seen in Figure 3, Ogden model can match well the material mechanics performance. When $N = 3$, the fitting parameters is shown in Table I.

In the case of several typical states, in Table II, the relationships of SED and CED are calculated along with the changes of θ and λ through the approach in this paper. As shown in Figures 4, 6, 7, and 8, θ is the angle of the crack plane normal vector with the first principal stretch direction; λ_1 is the first principal stretch ratio; $\frac{W_c}{W}$ is the ratio of CED and SED along with the changes of θ and λ_1, where W_c is the SED which is actually applied to create the first crack in the virgin sheet and W is the spent total SED.

Different from Mars and Fatemi[1] and Wang *et al.*,[20] the definition of biaxial parameter is the same with that of Zine *et al.*,[11] which aims to avoid the calculation inconvenience due to the introduction of logarithm in this study. Meanwhile, this study takes into account the effect of the changes of biaxial parameters β as the first principal stretch ratio in the calculation process.

The Analysis of CED Characteristics under Several Typical Strain States

In Figure 4, when $N = 3$, under uniaxial tension(UT), if $\theta=\pm\frac{\pi}{2}$, $W_c=0$; if $\theta=0$ or $\theta=\pm\pi$, $\frac{W_c}{W}$ has the maximum value 1,

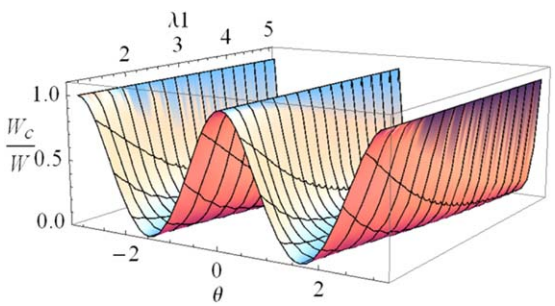

Figure 4. Variation of $\frac{W_c}{W}$ for UT under finite strain conditions. [Color figure can be viewed at wileyonlinelibrary.com.]

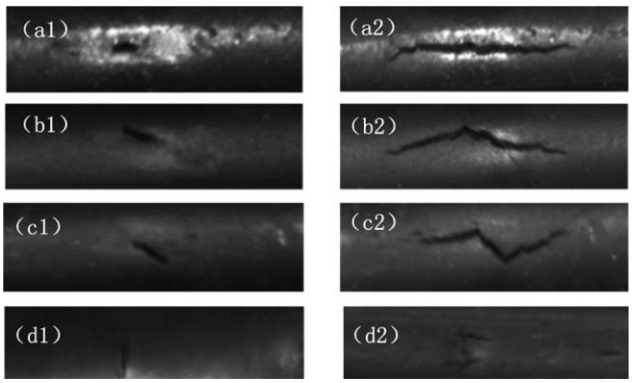

Figure 5. The fatigue crack propagation surface morphology of defects.

and the CED has the maximum value $W_{c,\max}=W$, which means all the strain energy density is available for the crack propagation when the maximum principal stretch direction and the crack plane are vertical. This shows that the potential crack direction is perpendicular to the maximum principal stretch under uniaxial stress state. The propagation surface morphology of uniaxial fatigue crack defects also confirms this feature in Figure 5. The initial crack orientation angle θ is gradually increases from 0° to 90°. Figure 5(a1,b1,c1,d1) are the propagation surface morphology before the deformation and Figure 5(a2, b2, c2, d2) are the corresponding propagation surface morphology after the deformation.

In Figure 6, under planar tensile/pure shear (PT/PS), the conclusions can be obtained as follows. When $\theta=0$ or $\theta=\pm\pi$, $\frac{W_c}{W}$ has the maximum value, and $\left(\frac{W_c}{W}\right)_{\max}=1$. When $\theta=\pm\frac{\pi}{2}$, $\frac{W_c}{W}$ has the minimum value, and with the increase of λ_1, the minimum value gradually tends to zero. This suggests that PT/PS will gradually be equivalent to UT with the increase of λ_1.

Under simple shear (SS), as shown in Figure 7, when $\theta=0$ or $\theta=\pm\pi$, $\frac{W_c}{W}$ has the maximum value; when $\theta=\pm\frac{\pi}{2}$, $\frac{W_c}{W}$ has the minimum value. With the increase of λ_1, $\left(\frac{W_c}{W}\right)_{\min}$ gradually tends to zero and $\left(\frac{W_c}{W}\right)_{\max}$ gradually tends to 1. This suggests that SS will also gradually be equivalent to UT with the increase of λ_1.

Under equal biaxial loading, in Figure 8 $\frac{W_c}{W}$ is independent of θ; $\frac{W_c}{W}$ identically equal to 0.5. It means the probabilities of the crack propagation in all directions are the same. Crack can be

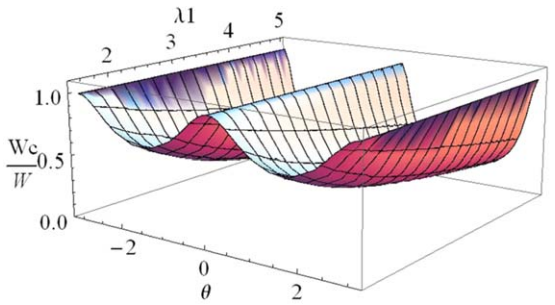

Figure 6. Variation of $\frac{W_c}{W}$ for PT/PS under finite strain conditions. [Color figure can be viewed at wileyonlinelibrary.com.]

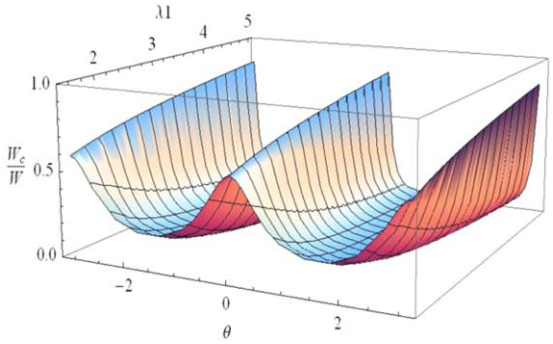

Figure 7. Variation of $\frac{W_c}{W}$ for SS under finite strain conditions. [Color figure can be viewed at wileyonlinelibrary.com.]

extended along arbitrary direction. So in any direction, not all of the SED will be used to drive the crack propagation. The result is consistent with Mars and Zine *et al.*[5,11]

Figures 4, 6, and 7 show $\frac{W_c}{W}$ presents periodic variation with the crack orientation angle θ. We just need to study the change of $\frac{W_c}{W}$ in $-\frac{\pi}{2} \le \theta \le \frac{\pi}{2}$. Under several typical strain conditions but equal biaxial loading, when $N=3$, $\lambda_1=1.5, -\frac{\pi}{2} \le \theta \le \frac{\pi}{2}$, $\frac{W_c}{W}$ changes with θ and it is symmetrical about θ=0 as shown in Figure 9. If $\theta = 0$, the CED has the maximum value $W_{c,\max}$.

For a given value λ_1, when N takes 4, 5, and 6, respectively, the relationships between SED and CED along with the change of θ and λ_1 are calculated. Their trends are the same when $N=3$ under uniaxial tension, as shown in Figure 10.

THE CED APPLICATION IN FATIGUE LIFE ESTIMATIONS

The validity of the CED method will be verified in rubber fatigue life prediction. By the calculation method of this article, the rubber fatigue life N_{f,W_c} is obtained based on the CED criterion of Ogden model. The results are compared with the SED method $N_{f,W}$ and the experimental values $N_{f,\exp}$.

The crack propagation rate $\frac{da}{dN}$ depends on the tearing energy T and corresponding material parameters A and F_0[13]:

$$\frac{da}{dN} = AT^{F_0}, \quad T_t \le T < T_c \tag{19}$$

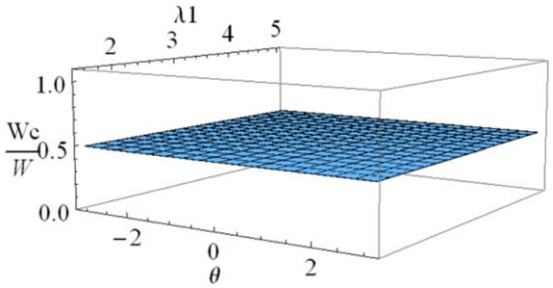

Figure 8. Variation of $\frac{W_c}{W}$ for equal biaxial loading under finite strain conditions. [Color figure can be viewed at wileyonlinelibrary.com.]

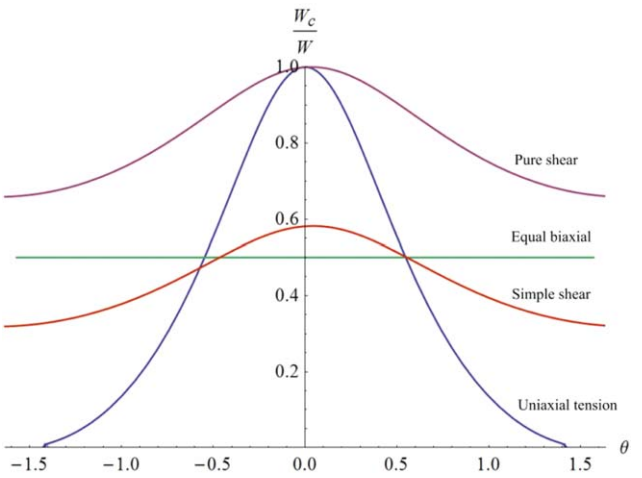

Figure 9. $N=3$, $\lambda_1=1.5$, the $\frac{W_c}{W}$ under several typical strain conditions. [Color figure can be viewed at wileyonlinelibrary.com.]

$$T = -\frac{dU}{dS} = 2k\mathrm{Wa} \tag{20}$$

The energy release rate is simply the change in the stored mechanical energy dU, per unit change in crack surface area dS. The correlation coefficient of strain level k is given in terms of the engineering strain $\varepsilon_{\max}$ by Lindley:

$$k = \frac{2.95 - 0.08\varepsilon_{\max}}{(1+\varepsilon_{\max})^{1/2}} \tag{21}$$

The material constant values are determined from experiments and are obtained as follows, by using the least square method according to eq. (19):

$$r_c = 4.85083 \times 10^{-5}\ \mathrm{m\ cycle}^{-1};$$
$$F_0 = 2.3034;$$
$$k = 1.74886;$$

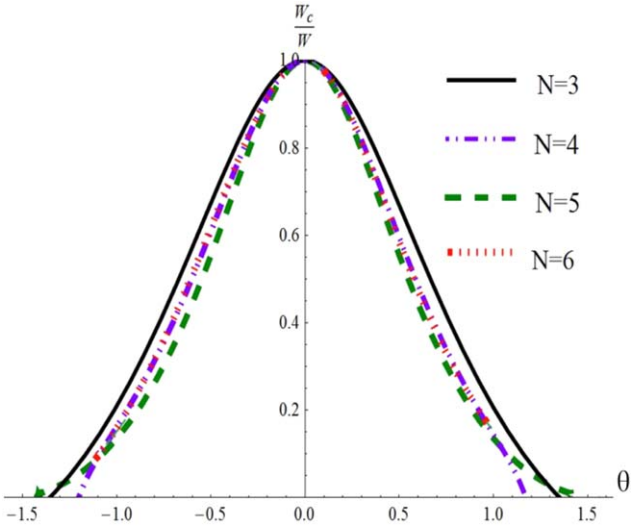

Figure 10. Variation of $\frac{W_c}{W}$ for UT when N = 3,4,5,6, $\lambda_1=1.5$. [Color figure can be viewed at wileyonlinelibrary.com.]

Table III. The Loading Conditions and Fatigue Lives

Loading case	Δa (mm)	θ (°)	$N_{f,W}$ (10^5cycle)	N_{f,W_c} (10^5cycle)	$N_{f,exp}$ (10^5cycle)	Scatter factor	
						$N_{f,w}/N_{f,exp}$	$\frac{N_{f,W_c}}{N_{exp}}$
1	0	90	—	—	5	—	—
2	0.08	52	0.161	4.529	5	1/31.06	1/1.04
3	1.80	20	1.459	2.643	3	1/2.06	1/1.14
4	1.91	20	2.817	5.106	5	1/1.77	1/0.98
5	0.17	45	0.368	4.894	4	1/10.87	1/0.82
6	0.60	25	1.307	3.404	4	1/3.06	1/1.18
7	1.94	3	2.916	2.984	3.5	1/1.20	1/1.17
8	0.44	30	0.579	2.158	2.5	1/4.32	1/1.16
9	3.84	15	0.979	1.314	2	1/2.04	1/1.52

$$T_c = 33.155 \text{ kJ m}^{-2}.$$

The critical crack propagation rate and critical tearing energy must satisfy:

$$r_c = AT_c^{F_0} \tag{22}$$

Substituting eq. (20) into eq. (19) an integral expression of N_f is calculated as eq. (23):

$$N_f = \int_{a_0}^{a_f} \frac{1}{A(2k\text{Wa})^{F_0}} \mathrm{d}a = \frac{1}{F_0 - 1} \frac{1}{A(2kW)^{F_0}} \left[\frac{1}{a_0^{F_0-1}} - \frac{1}{a_f^{F_0-1}} \right] \tag{23}$$

Hence, the predicted fatigue life of CED is expressed as follows:

$$N_{f,W_c} = \frac{N_{f,W}}{\left(\frac{W_c}{W}\right)^{F_0}} \tag{24}$$

The crack propagation tests of pure shear specimens were carried out in 25°C. The sizes of crack propagation were recorded using gray scale camera. The tests were terminated when multiple cracks appeared or crack propagation direction changed. A comparison between the measured lives and predicted fatigue lives based on the SED damage parameter and the CED damage parameter is shown in Table III. In Figure 11, all the predicted lives of the CED damage parameter distribution are within the double dispersion factor. Figure 11 and Table III reflect that the rubber fatigue life is clearly of great relevance to the crack orientation angle θ. It is meaningless to ignore the relationship between the crack plane normal vector and the maximum principal stretch direction in the study of crack propagation. When $\theta \neq 0$ and $\theta \neq \frac{\pi}{2}$, during the fatigue process, crack propagation rate will accelerate and θ will gradually be smaller, meanwhile, the crack plane and the maximum principal stretch direction will show a development trend which is perpendicular to each other. It verifies the conclusion that the potential crack direction is perpendicular to the maximum principal stretch.

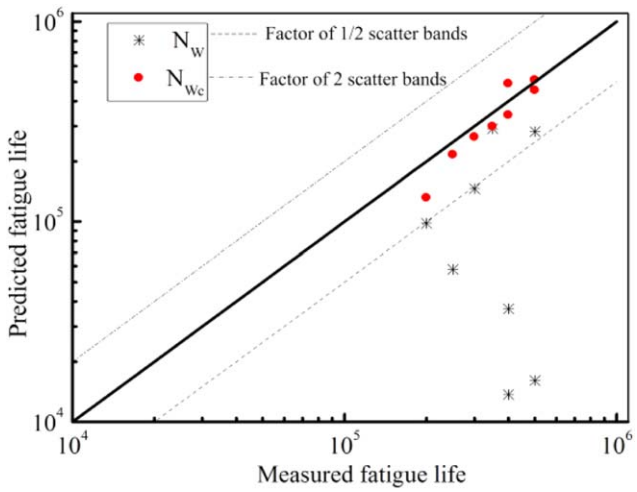

Figure 11. Comparison between SED and CED fatigue lives under pure shear. [Color figure can be viewed at wileyonlinelibrary.com.]

CONCLUSIONS

In this work, considering that the relationship between the fatigue life and the damage parameters which is a material property of the rubber fatigue can be considered independent on the geometry. The relationships between the principal stretch direction and crack surface normal have been concerned and investigated. In future studies, this method might be used to simplify the structure of complicated rubber components in engineering.

The relationship between SED and CED of Ogden hyperelastic constitutive model and the influence of the Ogden model order to the ratio of CED and SED have been discussed. The method might be used for the study of other similar high-order models, such as Reduced-polynomial model.

The predicted life based on SED criterion and the relationships between CED and SED are used to estimate the fatigue life of rubber based on CED criterion. The predicted values are compared with the measured values. While the angle between the crack plane normal vector and the first principal stretch direction is confirmed, the predicted fatigue lives based on the CED damage parameter are in excellent agreement with the experimental observations in a factor of two. The CED criterion is more suitable as a damage parameter to estimate the rubber material crack propagation under multiaxial loading.

ACKNOWLEDGMENTS

The authors gratefully acknowledge the financial support of the Guangdong and Hong Kong Project of Generic Technology (Project No. 2013B010134008) and the Science and Technology Program of Guangzhou (201509010008). We thank the editors and reviewers for their helpful and valuable comments.

REFERENCES

1. Mars, W. V.; Fatemi, A. *Rubber Chem. Technol.* **2004**, *77*, 392.
2. Zine, A.; Benseddiq, N.; Abdelaziz, M. N. *Int. J. Fatigue* **2011**, *33*, 1360.
3. Mars, W. V. *Rubber Chem. Technol.* **2007**, *80*, 481.
4. Ayoub, G.; Nait-Abdelaziz, M.; Zairi, F. *Int. J. Fatigue* **2014**, *66*, 168.
5. Mars, W. V. *Rubber Chem. Technol.* **2002**, *75*, 1.
6. Bahreman, M.; Darijani, H. *J. Appl. Polym. Sci.* **2015**, *132*, DOI: 10.1002/app.41718.
7. Ning, N. Y.; Zheng, Z. P.; Zhang, L. Q.; Tian, M. *Express Polym. Lett.* **2015**, *9*, 490.
8. Ovalle Rodas, C.; Zairi, F.; Nait-Abdelaziz, M. *J. Mech. Phys. Solids* **2014**, *64*, 396.
9. Zarrin-Ghalami, T.; Fatemi, A. *Fatigue Fract. Eng. Mater. Struct.* **2013**, *36*, 270.
10. Saintier, N.; Cailletaud, G.; Piques, R. *Int. J. Fatigue* **2006**, *28*, 61.
11. Zine, A.; Benseddiq, N.; Abdelaziz, M. N.; Hocine, N. A.; Bouami, D. *Fatigue Fract. Eng. Mater. Struct.* **2006**, *29*, 267.
12. Harbour, R. J.; Fatemi, A.; Mars, W. V. *J. Mater. Sci.* **2008**, *43*, 1783.
13. Mars, W. V.; Fatemi, A. *Int. J. Fatigue* **2002**, *24*, 949.
14. Benkahla, J.; Baranger, T. N.; Issartel, J. *Exp. Mech.* **2013**, *53*, 1383.
15. Arruda, E. M.; Boyce, M. C. *Int. J. Plast.* **1993**, *9*, 697.
16. Yeoh, O. H. *Rubber Chem. Technol.* **1997**, *70*, 175.
17. Twizell, E. H.; Ogden, R. W. *J. Aust. Math. Soc. B* **1997**, *24*, 424.
18. Kim, B.; Lee, S. B.; Lee, J. *Int. J. Precis. Eng. Man.* **2012**, *13*, 759.
19. Pulla, S. S.; Souri, M.; Karaca, H. E.; Lu, Y. C. *J. Appl. Polym. Sci.* **2015**, *132*, DOI: 10.1002/app.41861.
20. Wang, X. L.; Shangguan, W. B.; Li, M. M.; Duan, X. C.; Yan, J. *Eng. Mech.* **2015**, *32*, 197.
21. Shangguan, W. B.; Wang, X. L.; Deng, J. X. *Mater. Des.* **2014**, *58*, 65.
22. Lemaitre, J. *Meccanics* **2001**, *36*, 13.